# Stimulated hyper-Raman adiabatic passage. III. Experiment

K. Böhmer, T. Halfmann, L. P. Yatsenko,* B. W. Shore,† and K. Bergmann
*Fachbereich Physik der Universität, 67653 Kaiserslautern, Germany*
(Received 31 October 2000; published 2 July 2001)

We report the experimental realization of coherent population transfer from the $2\,^3S$ state to $2\,^3P$ fine-structure levels of helium, using the technique of hyper-Raman adiabatic passage, in which the pump-laser coupling involves a two-photon transition. We discuss the dependence of population transfer upon pump and Stokes detunings, and show that by suitably setting the detunings one can transfer population efficiently as either a two-step process to final states or as a single-step two-photon transition to an intermediate state. We use an adiabatic-state picture to interpret these experimental results. Since the optimum detuning depends on the pump laser intensity the transfer efficiency is compromised by the variation of the intensity across the spatial profile of the laser beam. Our experimental data agree well with numerical simulation based on density-matrix equations, including all 15 magnetic sublevels.

DOI: 10.1103/PhysRevA.64.023404 PACS number(s): 42.50.Ct, 32.80.Rm, 32.80.Qk, 42.50.Hz

## I. INTRODUCTION

Coherent population transfer via the stimulated Raman adiabatic passage method (STIRAP) [1] allows efficient and selective population transfer into a specific excited state in an atom or molecule. In this technique two laser pulses (pump and Stokes), timed in counterintuitive sequence of Stokes preceding pump pulse, couple the initial state to the target state via a Raman-type linkage through an intermediate (initially unpopulated) state. If the pulse shapes and pulse energies meet certain general conditions it is possible to transfer 100% of the population into the target state, and to do so without populating the intermediate state. The STIRAP method has been demonstrated experimentally for atoms and molecules using cw [1,2] as well as pulsed lasers [3–5].

In previous applications of STIRAP, both the pump and the Stokes couplings were one-photon transitions. For many molecules of interest the coupling to the first electronically excited state requires relatively short-wavelength pump photons (UV or vacuum ultraviolet). Sufficiently intense radiation sources for this spectral region suffer usually from poor coherence properties. The need for short-wavelength photons can be avoided when a two-photon transition is used for the pump excitation [6]. That is, the usual (1+1) Raman coupling scheme (one pump photon $\omega_p$, one Stokes photon $\omega_S$) is modified to a (2+1) hyper-Raman coupling scheme (two pump photons, one Stokes photon). The relatively high intensity required for the two-photon transition usually requires pulsed lasers.

Although the two-photon linkage permits use of longer-wavelength light, complications arise from unavoidable dynamic Stark shifts. These have been discussed theoretically in two earlier papers, referred to as paper I [7] and II [8]. The main problem, induced by the relatively intense pump pulse, is that the dynamic Stark shifts lead to a time-dependent detuning. If the two laser frequencies are initially tuned to two-step resonance $[2\omega_P-\omega_S=(E_f-E_i)/\hbar]$ with respect to the initial- and final-state energies, $E_i$ and $E_f$, respectively, this resonance condition cannot be maintained throughout the interaction and therefore the well-known dark state [1] will not exist at all times. The efficiency of the traditional STIRAP process relies on the continued existence of a dark state. Therefore the lack of such a state can hinder the transfer process. Furthermore one-photon ionization of the intermediate or final states may be a problem, if the ionization energy of these levels is less than $\hbar\omega_P$ or $\hbar\omega_S$.

In paper II we have shown that it is possible to maximize the transfer efficiency when the time-dependent detuning is partially compensated by an appropriate static detuning of pump and Stokes lasers (i.e., when the carrier frequencies of the pulses are suitably chosen). With this approach a dark state does not exist throughout the interaction and so some transient population reaches the intermediate state. Therefore a high transfer efficiency can be achieved only if the decay rate $\Gamma_{sp}$ out of the intermediate state is sufficiently small, $\Gamma_{sp}<T^{-1}$, where $T$ is the interaction time.

In this article we describe the experimental implementation of the stimulated hyper-Raman adiabatic passage (STIHRAP) technique using metastable helium as an illustrative example. The paper is organized as follows. In Sec. II we describe the radiative coupling scheme, the laser system, and the experimental apparatus. In Sec. III we present experimental data and compare the measured line shape to results from numerical simulations. In Sec. IV we use adiabatic states to interpret these results. We also use the semidiabatic states of paper II to discuss the pulse conditions that allow connection of the initial state to the target state.

## II. EXPERIMENT

### A. Atomic couplings

Figure 1 shows the triplet energy levels of metastable helium. The two-photon pump transition, together with the Stokes transition, form a $\Lambda$-type hyper-Raman coupling. Two pump photons of wavelength 855 nm couple the metastable initial state $2\,^3S$ to the intermediate state $3\,^3S$, and one

*Permanent address: Institute of Physics, Ukranian Academy of Sciences, Prospect Nauki 46, Kiev-22, 252650, Ukraine.
†Permanent address: Lawrence Livermore National Laboratory, Livermore, CA 94550.

 

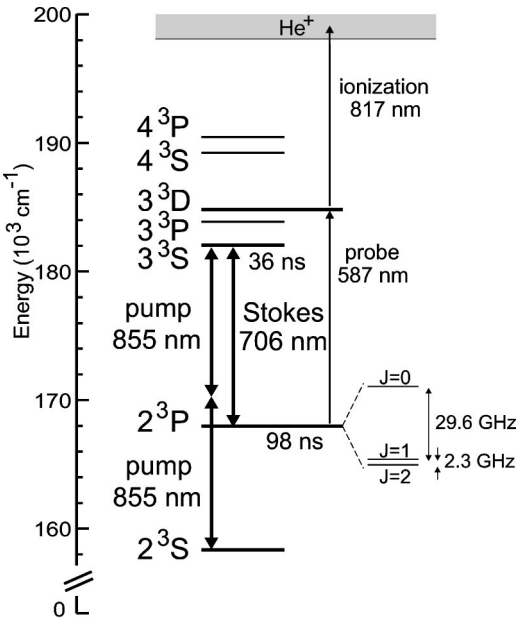


FIG. 1. Energy levels of the triplet manifold of metastable helium showing two-photon pump linkage, one-photon Stokes linkage, weak probe laser, and strong ionization laser.

Stokes photon at 706 nm couples the $3\,^3S$ state to the target state $2\,^3P$. None of the states involved can be ionized by one pump photon. The Stark shifts induced by the pump laser are of the order of magnitude of the effective two-photon Rabi frequency. The intermediate state lifetime is 36 ns (much longer than the 4.9-ns pulse duration) so that there are no significant losses by spontaneous decay during the interaction time. We note that the target state is not metastable, so there are losses before probing of the transferred population takes place. Its lifetime of 98 ns is long enough to permit buildup of coherence during the pulse duration and so to avoid detrimental effects on the transfer process.

Three different fine-structure levels can be chosen as target states. The Stokes couplings between the magnetic sublevels depend on the $J$ value of the target state (see Fig. 2). For $J=0$ the advantage is that it is well separated from adjacent states and that the STIHRAP process for $M=0$ takes

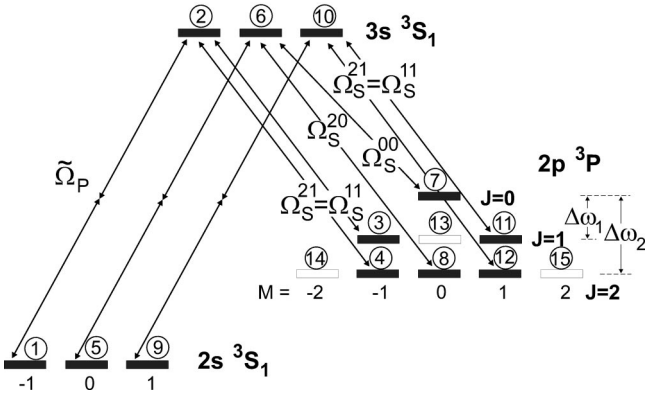


FIG. 2. Pump and Stokes couplings between the magnetic sublevels for linearly polarized light. Encircled numbers show our indexing scheme (see the Appendix).

TABLE I. Calculated values of Rabi frequencies and dynamic Stark shifts induced by the pump laser, in units of angular frequency (rad/s). Intensities of pump ($I_P$) and Stokes ($I_S$) laser in W/cm$^2$.

| State | Shift | Rabi frequency |
|---|---|---|
| $2\,^3S_1$ | $141I_P$ | |
| $3\,^3S_1$ | $118I_P$ | $\tilde{\Omega}_P=152I_P$ |
| $2\,^3P_0$ | $-143I_P$ | $\Omega_S^{00}=1.61\cdot10^8\sqrt{I_S}$ |
| $2\,^3P_1,\ M=\pm1$ | $-209I_P$ | $\Omega_S^{11}=0.9\cdot10^8\sqrt{I_S}$ |
| $2\,^3P_2,\ M=0$ | $-220I_P$ | $\Omega_S^{20}=2.28\cdot10^8\sqrt{I_S}$ |
| $2\,^3P_2,\ M=\pm1$ | $-145I_P$ | $\Omega_S^{21}=0.9\cdot10^8\sqrt{I_S}$ |

place within a three-level system when the Stokes laser is tuned close to resonance with $J=0$. However, in the experiment all magnetic sublevels in the initial state are populated and coupled to the intermediate state, but the $M=\pm1$ sublevels of the intermediate state are not coupled to the $J=0$ target state due to the selection rules for the Stokes transition (pump and Stokes laser are linearly polarized). This means that, although complete population transfer is possible within the system of the three coupled quantum states, no more than 33% of the entire population in the initial state can be transferred to the target state. For $J=1$ only the magnetic sublevels $M=\pm1$ are coupled to the target state. For $J=2$ all three magnetic sublevels are coupled. We focus attention on this case. Additional complications arise here because of the vicinity of the $J=1$ level and because of the dependence of the Stark shifts and Rabi frequencies on the value of $M$.

As shown in paper II the balance of the relevant Stark shifts and Rabi frequencies is crucial. Table I presents the basic parameters (Stark shifts and Rabi frequencies) that fill the Hamiltonian matrix for this system. These were calculated using a model-potential approach described in detail in Ref. [9].

### B. Lasers

The laser system is shown in Fig. 3. The pump pulse at 855 nm was produced by pulsed amplification of the cw output of a single-mode Ti:sapphire ring laser in a pulsed dye amplifier. The amplifier was pumped by the second harmonic of an injection-seeded *Q*-switched Nd:YAG (Yttrium Aluminum Garnet) laser (Spectra Physics GCR 4). The Stokes pulse was generated by amplifying the radiation at 706 nm from a cw single-mode ring dye laser in another pulsed dye amplifier also pumped by the second harmonic of the same Nd:YAG laser. Typical pulse energies were 1 mJ at 706 nm and up to 11 mJ at 855 nm; the duration of the pulses was 4.9 ns (full width at half maximum of laser intensity). The pulses were delayed by a variable optical delay line and spatially overlapped in the interaction region inside the detection chamber. Both laser beams were copropagating and had parallel linear polarization. The probe and ionization pulses (see Sec. II D) at 587 nm and 817 nm were generated in two different multimode dye lasers (Lambda Physik LPD 3000) pumped by the same excimer laser (Lambda Physik LPX 220). Typical pulse energies used were 1 mJ at 817 nm

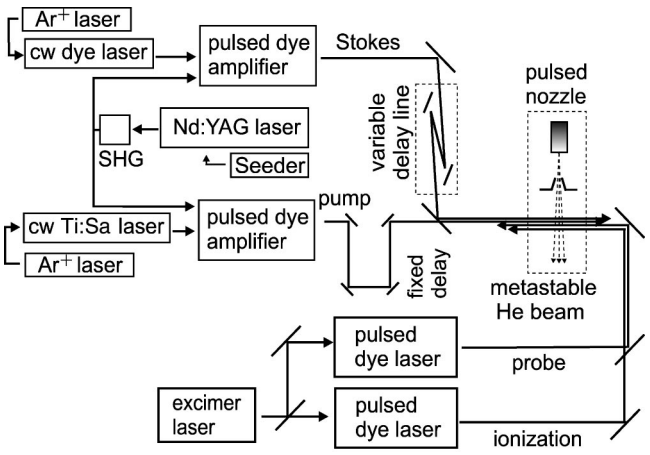


FIG. 3. Experimental setup. The pump and Stokes pulses are generated by pulse amplification of cw radiation, the probe and ionization pulses are produced by two excimer-pumped dye lasers.

and 30 $\mu$J at 587 nm. The probe- and ionization-laser beams were copropagating with respect to each other and antiparallel with respect to the STIHRAP lasers. Pump and ionization laser were slightly focused and the four laser beams spatially overlapped in the interaction region, where the beam radii (at $1/e$ of peak intensity) were about 0.6–1.0 mm for the pump beam, 6 mm for the Stokes beam, 0.8 mm for the ionization beam, and several mm for the probe beam.

### C. Metastable source

A pulsed beam of helium was expanded through a nozzle (general valve; opening diameter 0.8 mm) with a stagnation pressure of 1200 mbar. The atoms were excited from the ground state $1\,^1S$ to the metastable triplet state $2\,^3S$ by electron impact in a pulsed gas discharge that was injection seeded by a continuous current of electrons to strongly enhance the stability and efficiency. The discharge was operated 4 mm behind the nozzle. A skimmer (diameter 0.8 mm) was placed 40 mm away from the nozzle to collimate the atomic beam and to separate the source chamber from the region of interaction and detection. The metastable source is described in detail elsewhere [10].

### D. Detection scheme

The population in the target state $2\,^3P$ was detected by two-color resonant-enhanced multiphoton ionization 75 ns after the STIHRAP interaction. To detect helium-ions mass selectively we used a short time-of-flight segment terminated by a double-thickness microsphere plate (El Mul Technologies). The output current of the microsphere plate was amplified with fast broad-band amplifiers and was integrated in a boxcar-gated integrator (EG&G 4121 B).

In order to resolve the $J=0$ level from the $J=1,2$ levels a weak probe laser at 587 nm was used to excite the $3\,^3D$ state. From there the atoms were ionized by 817-nm photons. The excitation and ionization pulses overlapped in time. Depending on the frequency of the probe laser either the population in $J=0$ or in $J=1$ and $J=2$ was detected. The $J=1$ and $J=2$ levels could not be resolved; their separation of 2.3 GHz

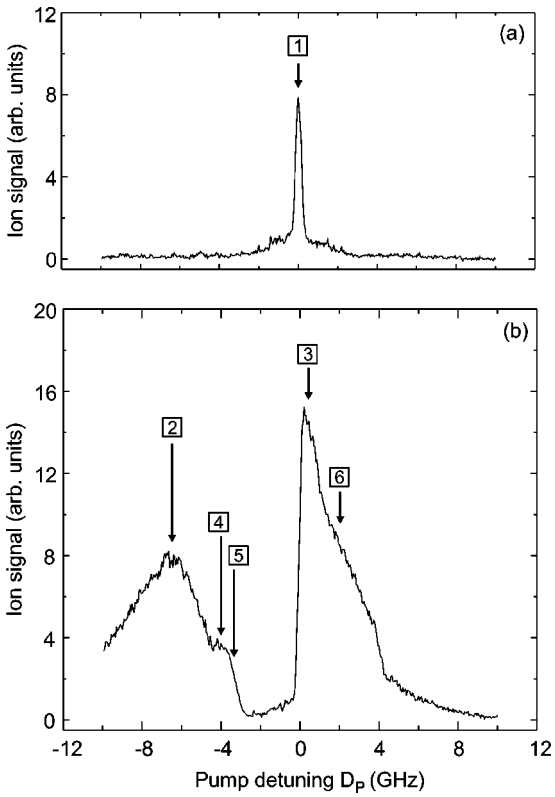


FIG. 4. Variation of the ion signal as a function of the pump-laser frequency with the detection laser tuned to probe the population in the $J=1$ and $J=2$ target states. $I_P=200\,\mathrm{MW/cm^2}$, $I_S=0.21\,\mathrm{MW/cm^2}$, and $\Delta\tau=-3.3$ ns. (a) without Stokes laser, (b) with Stokes laser. The numbers in squares mark specific pump detunings for which we present the dependence of the ion signal on the probe-laser frequency (see Fig. 5) or calculated adiabatic states (see Figs. 9–11).

is within the 6-GHz bandwidth of the probe laser. Therefore the variation of the ion signal with the probe-laser frequency typically shows two peaks (see Sec. III A).

It is a specific feature of the chosen level scheme that the intermediate state $3\,^3S$ can decay to all fine-structure levels of $2\,^3P$ (in fact, these are the only radiative decay channels). As a consequence it is possible to simultaneously monitor the population in the target and the intermediate state after the STIHRAP process by tuning the probe-laser frequency across the resonance with the $3\,^3D$ state. If, for example, the Stokes laser induces population transfer to the $J=2$ level then all population in $J=0$ must originate from atoms that were excited to the intermediate state and decayed from there.

## III. RESULTS

### A. Line shape

The experimental detunings are defined as follows. The pump detuning $D_P=\nu_P-(E_{3s}-E_{2s})/(2h)$ is the detuning of the pump-laser frequency $\nu_P$ from two-photon resonance with the $2\,^3S\leftrightarrow 3\,^3S$ transition. The Stokes detuning $D_S=\nu_S-(E_{3s}-E_{2p,J=1})/h$ is the detuning of the Stokes-laser frequency $\nu_S$ from the one-photon resonance with the $3\,^3S\leftrightarrow 2\,^3P_1$ transition.

Figure 4(a) shows the dependence of the ion signal on the pump-laser frequency with the Stokes laser blocked. The probe laser detects population in $J=1$ and $J=2$. When the pump laser is tuned to two-photon resonance ($D_P=0$) the ion signal originates from atoms that are excited to the $3\,^3S$ state and decay to the target states. Figure 5(a) shows the associated dependence of the ion signal on the frequency of the probe laser with the Stokes laser blocked. The ratio of the two peaks is determined by the values of the Einstein A coefficients for the transitions to the three fine structure levels.

Figure 4(b) shows the variation of the ion signal over the same pump frequency range with the Stokes laser on. The line shape changes dramatically. There are two peaks, one at negative and one at positive pump detuning. The associated dependence on the probe-laser frequency [Figs. 5(b) and 5(c)] reveals that — depending on the pump detuning — the Stokes laser induces two entirely different processes. When the pump laser is tuned to the peak at negative detuning [Fig. 5(b)] population is transferred to $J=2$ and the intermediate state is not populated, as verified by the disappearance of the ion signal out of the $J=0$ level. This is the STIHRAP process. We note that there will always be *transient* population in the intermediate state as discussed in paper II, but this is not detected when probing after the STIHRAP interaction. When the pump laser is tuned to the peak at positive detuning [Fig. 5(c)] the probe laser-induced ionization from $J=0$ and $J=1,2$ is enhanced. This indicates a Stokes laser-induced efficient population transfer to the intermediate state from where the atoms decay to all target levels.

The experimental results are nicely reproduced by a numerical simulation of the system (see the Appendix). Figures 6(a) and 6(b) show the calculated population in the target states and the intermediate state immediately after the STIHRAP interaction (5 ns after the pump pulse). For a pump detuning of $D_P=-6.5$ GHz the $J=2$ target state is efficiently populated [Fig. 6(a)], for $D_P=+0.3$ GHz about 85% of the population is in the intermediate state [Fig. 6(b)]. Figure 6(c) shows the sum of the population in the $J=1$ and $J=2$ target states at the time of probing (75 ns after the pump pulse). As compared to Fig. 6(a) the population transferred by STIHRAP (at $D_P=-6.5$ GHz) has decreased due to the finite lifetime of the target state; the population at positive pump detuning originates from the intermediate-state population [see Fig. 6(b)] that has decayed into the much longer lived target states.

The position of the STIHRAP peak is as expected from the discussion in paper II: Depending on the value of the dynamic Stark shift there exist static pump and Stokes detunings so that population transfer to the target state is successful. The optimal choice of the pump frequency is power dependent and does not coincide with either the two-photon resonance condition ($D_P=0$) or the (2+1)-resonance condition.

The process of efficient population of the intermediate state was not discussed in paper II because there attention was focused on the target state. The fact that this process appears as a dominant feature in the data presented here is due to a particular property of the chosen level scheme: the strong decay from the intermediate state to the target state. This process is similar to the Stark chirped rapid adiabatic passage (SCRAP) [11]. In that scheme efficient population transfer to the intermediate state is induced by Stark shifting the energy separation $\Delta E_{1,2}$ of the initial and intermediate state through resonances with the energy of two pump-laser photons while the pump-laser intensity is high. At this time the population is transferred to the upper state by adiabatic passage. The energy $\Delta E_{1,2}$ is swept again through the reso-

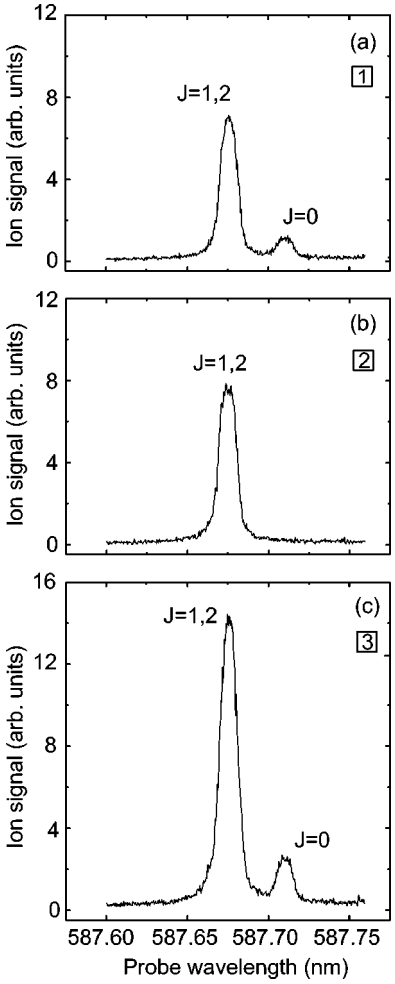


FIG. 5. Variation of the ion signal as a function of the probe wavelength for three different pump detunings marked by numbers in squares in Fig. 4. The detuning of the Stokes laser is fixed. The probe laser is scanned across the one-photon resonance with the $2\,^3P$-$3\,^3D$ transition. The height of the peaks is a direct measure for the population in the fine-structure levels of the target state. $J=1$ cannot be resolved from $J=2$. The probe-laser wavelength is accurate to within $\pm 0.08$ nm. (a) The pump-laser frequency is tuned to $D_P \simeq 0$ (see text), the Stokes laser is blocked. The population of the target state is generated by spontaneous decay of the intermediate state. (b) The pump-laser frequency is tuned to $D_P=-6.5$ GHz. Population is transferred to the $J=2$ target state via STIHRAP. The intermediate state is not populated, the signal from the $J=0$ target state disappears. (c) The pump-laser frequency is tuned to $D_P=+0.3$ GHz. The intermediate state is efficiently populated, the signal in all target state levels is enhanced.

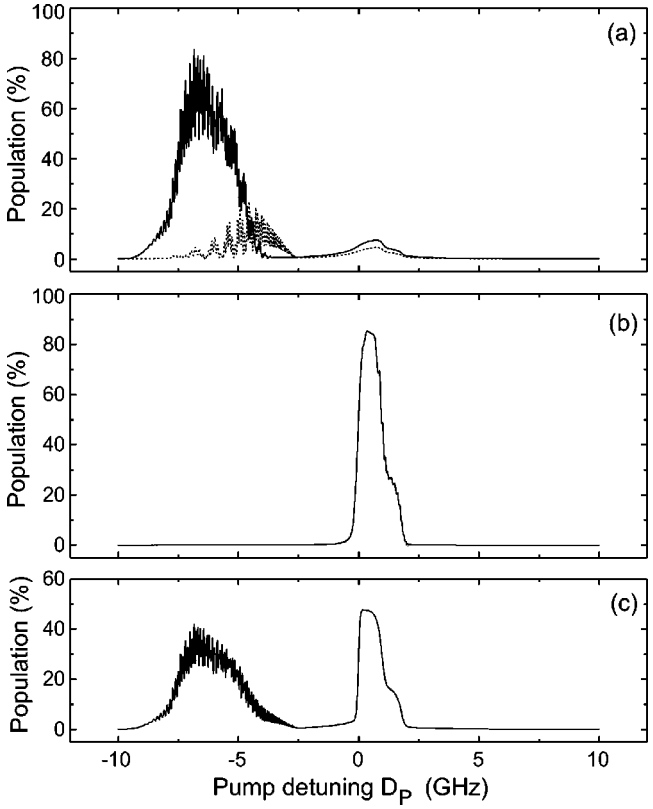


FIG. 6. Numerical simulation of the population as a function of the pump detuning for the parameters of Fig. 4(b). For negative pump detuning the population is mainly transferred to the target state (STIHRAP), for positive pump detuning the intermediate state is efficiently populated. The fast oscillations of the target-state populations are caused by the interference of two possible ways of population transfer due to nonadiabaticity. (a) Population in the target states 5 ns after the interaction with the STIHRAP lasers. Solid line: $2\,^3P_2$, dashed line: $2\,^3P_1$. (b) Population in the intermediate state ($3\,^3S$) 5 ns after the interaction. (c) Sum of the population in the target states $2\,^3P_2$ and $2\,^3P_1$ at the time of probing, 75 ns after the interaction with the STIHRAP lasers. The population at positive pump detuning is generated by spontaneous decay from the intermediate state. This frame models the experimental lineshape shown in Fig. 4(b).

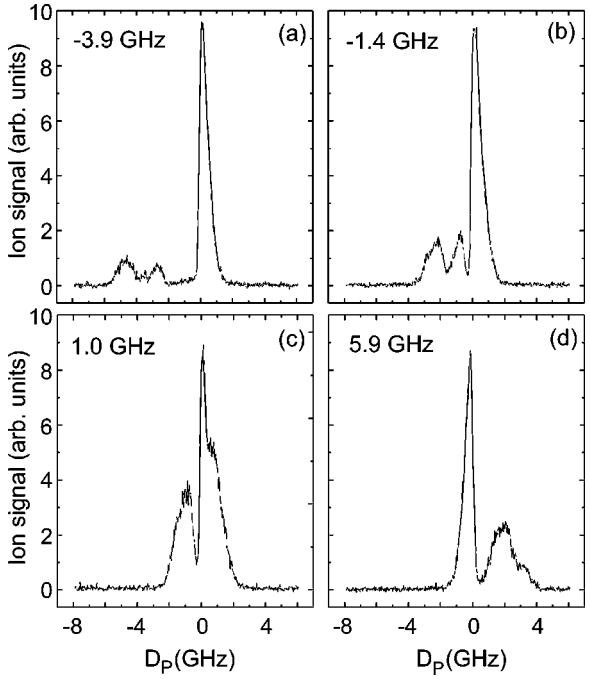


FIG. 7. Variation of the ion signal depending on the pump laser frequency for four different Stokes detunings $D_S$ (indicated in the upper left corner). $I_P=80$ MW/cm$^2$ and $I_S=0.04$ MW/cm$^2$, $\Delta\tau=-5$ ns. The population in $2\,^3P$ $J=1$ and $J=2$ is detected. The line shapes strongly depend on the value of the Stokes detuning and can be explained as horizontal intersections through the connectivity plot (Fig. 12).

nance, as the intensity of the Stark shift laser decreases, when the pump-laser intensity is small or zero. Therefore, the reverse process, adiabatic passage to the ground state, does not occur. In the case observed here the efficient population transfer to the intermediate state does *not* require an additional, strong, Stark shifting laser.

Both processes can be understood by investigating the adiabatic energies (see Sec. IV A).

### B. Transfer efficiency

The transfer efficiency is calculated by comparing the detection signal from the target state in STIHRAP configuration (Stokes laser on) with the detection signal when the Stokes laser is blocked and the pump laser is tuned to resonance with the pump transition. If the target state is metastable, this enhancement can be directly converted to population transfer [3]. In the case discussed here the finite lifetime of the target state (98 ns) has to be taken into account: even if the target state is efficiently populated some fraction of the population will be lost between the end of the STIHRAP interaction and the arrival of the probe pulse. The evolution of the population during this time interval when no lasers are present is described by a set of differential equations for level populations coupled due to spontaneous decay. These can be solved analytically [see Eqs. (1) and (2)]. The population in the target state is probed 75 ns after the pump pulse. From this value we calculate the population that was in the target state immediately after the STIHRAP interaction.

If at $t=t_{end}$ the population in state $i$ is denoted by $N_i^0$ and there is no further laser interaction then the population $N_i(t)$ at time $t$ is given by

$$N_2(t)=N_2^0 e^{-\Gamma_2 t'}, \tag{1}$$

$$N_{3J}(t)=\frac{\Gamma_{2\to 3J}}{\Gamma_2-\Gamma_{3J}}N_2^0(e^{-\Gamma_{3J}t'}-e^{-\Gamma_2 t'})+N_{3J}^0 e^{-\Gamma_{3J}t'}, \tag{2}$$

where $t'=t-t_{end}$. Here $\Gamma_i$ denotes the total decay rate of state $i$, $\Gamma_{2\to 3J}$ denotes the rate for the decay of the intermediate state into the $2\,^3P_J$ state. Our notation is $i=1$ for the initial state $2\,^3S$, $i=2$ for the intermediate state $3\,^3S$, and $i=3J$ for the target state $2\,^3P_J$.

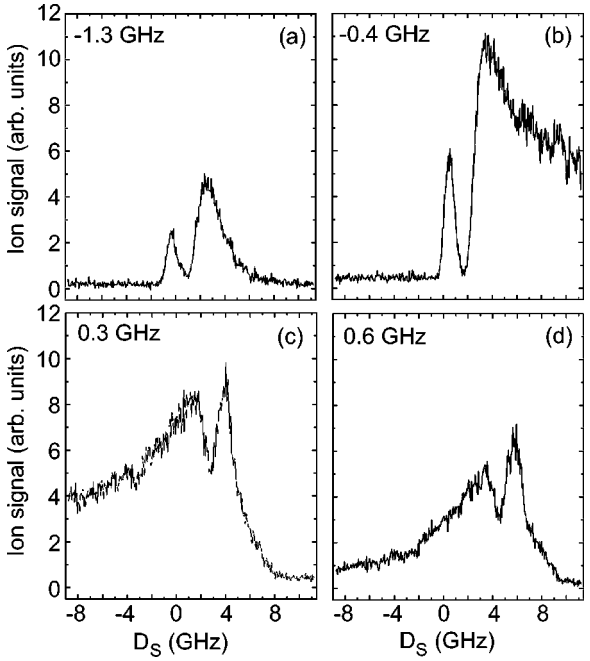


FIG. 8. Variation of the ion signal depending on the Stokes-laser frequency for four different pump detunings (indicated in the upper left corner). $I_P = 80$ MW/cm$^2$ and $I_S = 0.04$ MW/cm$^2$, $\Delta\tau = -5$ ns. The population in $2\,^3P$ $J=1$ and $J=2$ is detected. The line shapes strongly depend on the value of the pump detuning and can be explained as vertical intersections through the connectivity plot (Fig. 12).

Without the Stokes laser the intermediate state will be populated by the pump laser. If the transition is saturated then 50% of the population will be in the upper state after the interaction. [For coherent excitation the term ''saturation'' means that for sufficiently high Rabi frequencies averaging over the pulse amplitude fluctuations and over the spatial profile yields a 50% population of the upper state.] This population decays into the target state and from the target state back to the initial state. From Eq. (2) we calculate the fraction of the population that will reside in the $J=1$ and $J=2$ levels at the time of probing. This value corresponds to the ion signal from the $J=1$ and $J=2$ levels measured in Fig. 4(a) for $D_P = 0$.

The presence of the Stokes laser enhances the ion signal slightly [compare the peak at $D_P = -6.5$ GHz in Fig. 4(b)]. The enhancement yields the fraction of the population that is residing in the target states 75 ns after the STIHRAP interaction. Using again Eq. (2) we calculate the population that was placed in the target state immediately after the STIHRAP interaction. From the data shown in Fig. 4 we derive a transfer efficiency of $(53 \pm 5)\%$. The comparison of the maximum ion signal in Figs. 4(a) and 5(a) shows that the pump laser was slightly detuned (by about 80 MHz) from the two-photon resonance with the pump transition ($D_P = 0$) when the data shown in Fig. 5(a) were taken. Therefore those data must not be used for calibrating the transfer efficiency.

The deviation from 100% is due to the fact that the transfer efficiency is averaged over the spatial profile of the pump laser. The success of the transfer process is very sensitive to the intensity of the pump laser because the required static detunings depend on the value of the dynamic Stark shifts and these are proportional to intensity. For a power variation across the diameter of the pump beam it is not possible to have optimum parameters across the entire beam. Even if the transfer efficiency is 100% in the center of the pump beam there will be lower efficiency in the wings and the integrated efficiency will drop significantly.

We confirmed this by a numerical simulation. Assuming a

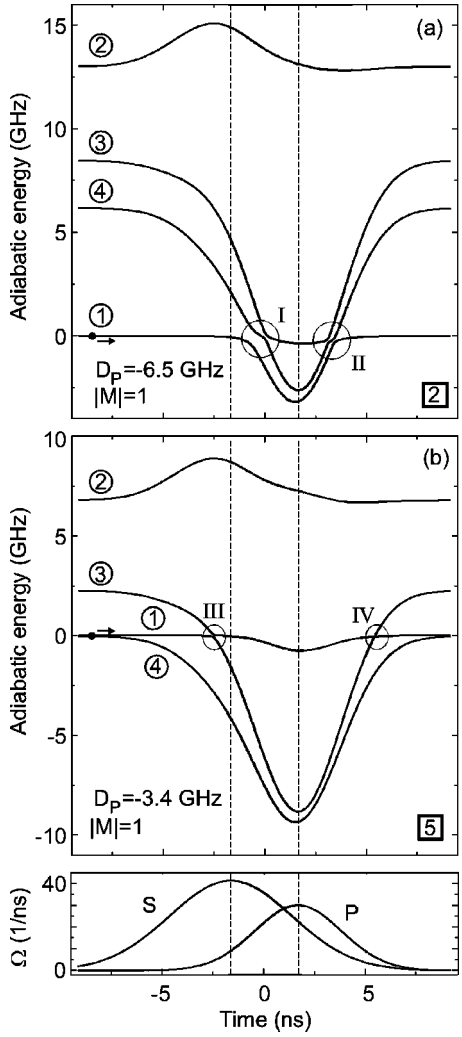


FIG. 9. Time evolution of the energies of the adiabatic states in the four-level system $2\,^3S_1$, $3\,^3S_1$, $2\,^3P_1$, $2\,^3P_2$ ($M=-1$) for various pump detunings as marked by numbers in squares in Fig. 4(b). The Stokes detuning is kept fixed at $D_S = -4.5$ GHz. The numbers in circles (compare Fig. 2) to the left side of the curves denote the bare state to which the adiabatic states connect when both lasers are off. $I_P = 200$ MW/cm$^2$, $I_S = 0.21$ MW/cm$^2$, and $\Delta\tau = -3.3$ ns. The vertical dashed lines indicate the peak values of the Rabi frequencies. (a) STIHRAP configuration. The population is transferred to the $J=2$ target state. Some population remains in the initial state. (b) Although the two-step resonance condition with respect to the initial state and the $J=2$ target state is fulfilled [one of the prerequisites for successful population transfer in conventional $(1+1)$ STIRAP] there is no efficient population transfer to $J=2$. (c) Pulse sequence.

Gaussian spatial profile $I(r)=I_0\exp(-r^2/w^2)$ for the pump laser and assuming that all atoms up to a radius of $0.95\,w$ are detected by the ionization laser, we decomposed the pump-laser profile into rings of equal intensities, ran the simulation (see the Appendix) for the intensities associated with every ring and averaged the resulting transfer efficiencies with their respective weights. For the static detunings used in the experiment, which yield an 84% transfer efficiency in the center of the pump beam, the averaged efficiency dropped to a value of 55%, which is in good agreement with our experimental data.

The sensitivity to laser intensity is one of the major differences to (1+1) STIRAP. In the latter case Stark shifts can be neglected, and it is sufficient to work with power levels that guarantee adiabatic evolution; power variations across the beam are not detrimental as long as the minimum power is above the adiabaticity limit.

### C. Sensitivity to detuning

As expected from paper II the process is extremely sensitive to the chosen values for the pump and Stokes detuning. Figure 7 shows the variation of the population transfer as a function of the pump detuning for different values of the Stokes detuning. Figure 8 shows the dependence on the Stokes detuning for various pump detunings. The resulting line shapes can be understood as intersections through a two-dimensional connectivity plot (see Sec. IV B).

## IV. DISCUSSION

### A. Analysis of population transfer using adiabatic states

The understanding of a multilevel system evolving in time under the influence of a time-dependent Hamiltonian can often be facilitated by viewing plots of diabatic energies (diagonal elements of the Hamiltonian matrix) and adiabatic energies (eigenvalues of the Hamiltonian) versus time: when adiabatic conditions hold, the statevector is aligned with one of the adiabatic eigenstates and follows an adiabatic curve through avoided crossings.

The line shape in Fig. 4(b) is discussed in the adiabatic state picture. As shown in Fig. 2 the system under consideration decomposes into three independent four-level systems: two identical systems for $M=\pm1$ and one for $M=0$. Figures 9–11 show the time evolution of the adiabatic energies in these four-level systems for several pump detunings marked in Fig. 4(b). The adiabatic states are labeled as in paper II: $\Phi_1(\Phi_2,\Phi_3,\Phi_4)$ denotes the adiabatic state that connects to the bare state $2\,^3S$ ($3\,^3S$, $2\,^3P_1$, $2\,^3P_2$). The ordering is such that during the process the relative order of adiabatic eigenvalues is unchanged. The index refers to the encircled numbers in Figs. 9–11. With this definition different adiabatic energy curves can touch (be degenerate), but cannot cross. The static detunings are revealed in the asymptotic behavior of the adiabatic energies. In all cases of Figs. 9–11 the population is initially in $\Phi_1$.

The two key features in Fig. 4(b), population transfer via STIHRAP and efficient population transfer to the intermediate state, will be discussed in Secs. IV A 1 and IV A 2. Further (minor) details of the line shape will be described in Sec. IV A 3.

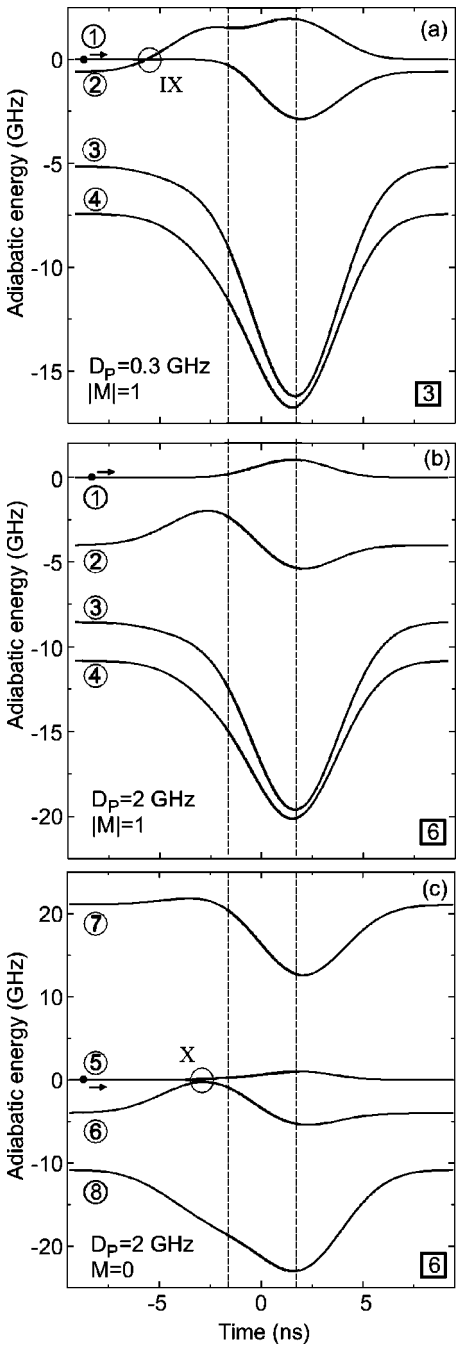


FIG. 10. The two independent four-level systems $2\,^3S_1$, $3\,^3S_1$, $2\,^3P_1$, and $2\,^3P_2$ for $M=-1$ and $2\,^3S_1$, $3\,^3S_1$, $2\,^3P_0$, and $2\,^3P_2$ for $M=0$ are considered. Parameters, labels, and pulse sequence as in Fig. 9. (a) Efficient population transfer to the intermediate state. (b) For $M=-1$ population remains in the initial state. (c) For $M=0$ there is still transfer to the intermediate state.

#### *1. STIHRAP*

The adiabatic states for the STIHRAP configuration [see the peak marked 2 at a pump detuning of $D_P=-6.5\,\mathrm{GHz}$ in Fig. 4(b)] are shown in Fig. 9(a). Initially, the population is

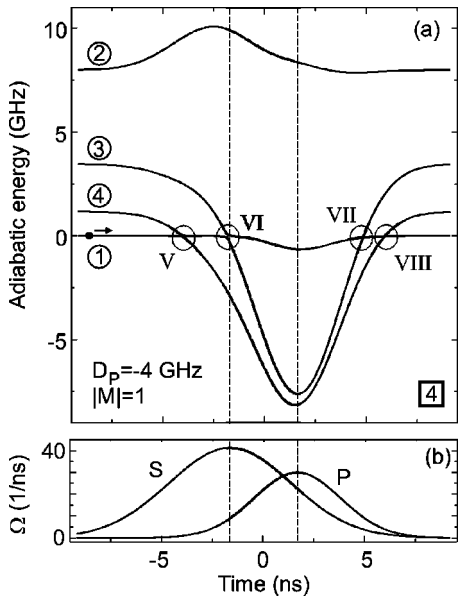


FIG. 11. Same as Fig. 9(a). The major part of the population remains in the initial state, some is transferred to $J=1$. (b) Pulse sequence.

in $\Phi_1$. At the avoided crossing I the eigenvalue of $\Phi_1$ is well separated from those of $\Phi_4$ and $\Phi_3$. Therefore the population remains in $\Phi_1$.

At the avoided crossing II the eigenvalues of $\Phi_1$ and $\Phi_4$ approach each other more closely. The diabatic transition required for population transfer may take place here. There is a nonvanishing probability for the population to remain in $\Phi_1$ or to make a transition to $\Phi_3$. During the entire process the eigenvalue of the adiabatic state $\Phi_2$ is far removed from that of $\Phi_1$. This means that even when the condition for adiabatic evolution is poorly fulfilled the intermediate state will not be populated. The adiabatic states for $D_P=-3.4\,\mathrm{GHz}$ (which corresponds to exact two-step resonance between the initial state and the $J=2$ target state) are displayed in Fig. 9(b), to illustrate that population transfer is *not* efficient for exact two-step resonance.

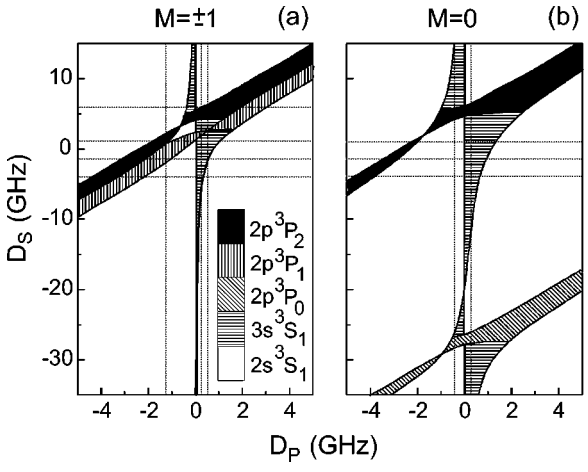


FIG. 12. Connectivity plot as a function of pump and Stokes detunings. $I_P=55$ MW/cm$^2$ and $I_S=0.03$ MW/cm$^2$. The shaded areas indicate the state that connects to the initial state. Dashed lines indicate detunings for which we present experimental data in Figs. 7 and 8.

At crossing III part of the population remains in $\Phi_1$, while part of the population makes a transition to $\Phi_3$. At crossing IV part of the population makes a transition from $\Phi_1$ to $\Phi_3$ and from $\Phi_3$ to $\Phi_1$. The remaining fraction will stay in their respective adiabatic states. There is no pathway for population transfer from $\Phi_1$ to $\Phi_4$. The signal for $D_P=-3.4\,\mathrm{GHz}$, see Fig. 4(b), is significantly smaller than at the STIHRAP peak. It originates from the fraction of population in $J=1$.

#### *2. Population transfer to the intermediate state*

The peak at $D_P=0.3\,\mathrm{GHz}$ in Fig. 4(b) originates from efficient population transfer to the intermediate state and subsequent decay to the target state. Figure 10(a) shows an early crossing (IX) between adiabatic states $\Phi_1$ and $\Phi_2$. In a diabatic transition nearly all population is transferred from $\Phi_1$ to $\Phi_2$ and is found in the intermediate state at the end of the process.

#### *3. Further details of the line shape*

The wing at the high-frequency side of the peak marked 3 in Fig. 4(b) shows some structure. This structure [marked 6 in Fig. 4(b)] is explained in Figs. 10(b) and 10(c). For $D_P=+2$ GHz the early diabatic transition for the $M=\pm1$ magnetic sublevels does not exist any more [see Fig. 10(b)]. However, for the same detuning this transition is still possible for $M=0$ [see Fig. 10(c), crossing $X$].

Figure 11(a) explains the structure in the wing at the high-frequency side of the STIHRAP peak shown in Fig. 4(b). Here $J=1$ is populated. The signal is much smaller than for $D_P=-6.5\,\mathrm{GHz}$; the major part of the population remains in the initial state. Here the evolution is along various pathways. At the avoided crossing V there is a diabatic transition from $\Phi_1$ to $\Phi_4$. While passing through the avoided crossing VI the probabilities to remain in $\Phi_4$ or to make a transition to $\Phi_3$ are both nonzero.

At the avoided crossing VII the population in $\Phi_3$ either remains in that state if the condition for adiabatic following is satisfied or it makes a diabatic transition to $\Phi_4$. The population that was in $\Phi_4$ between crossings VI and VII either remains there or makes a diabatic transition to $\Phi_3$.

Crossing VIII is an avoided crossing with very small spacing; there is a diabatic transition from $\Phi_4$ to $\Phi_1$. In this configuration many pathways are possible. The overall effect is a high probability for the population to remain in the initial state and a low probability for population transfer to $J=1$.

### B. Connectivity regions

At each moment there is a list of $N$ adiabatic eigenvectors, ranked by increasing energy. If the evolution is adiabatic, then always the state vector is aligned with the same adiabatic state, say the $n$th one. But the composition of these adiabatic states varies with time. If the evolution is *not* adiabatic then one must determine which adiabatic state is associated with the state vector after a nonadiabatic interval.

The connection between prior- and post-adiabatic states, around a time interval during which the evolution is not adiabatic, we refer to as *connectivity*.

In paper II we showed that it is often useful to consider ''semidiabatic'' energies, which are obtained by considering the action of only one of the two laser pulses. In this approach adiabatic evolution is required during the time between pulse maxima (*peak-to-peak connectivity*) while diabatic evolution is assumed for times earlier and later than pulse maxima, despite the presence of both pulses during this time.

The level scheme used in our experiment is more complicated than the three-level case considered in paper II. As was already mentioned, the system under consideration consists of three independent *four*-level systems: two identical systems for $M=\pm 1$ ($2\,^3S_1$, $3\,^3S_1$, $2\,^3P_1$, and $2\,^3P_2$) and one system for $M=0$ ($2\,^3S_1$, $3\,^3S_1$, $2\,^3P_0$, and $2\,^3P_2$). Thus, we have to consider two independent plots of connectivity regions (for $M=\pm 1$ and for $M=0$). The procedure is as follows.

Consider for example the system for $M=-1$. We are interested in the Stokes semi-diabatic eigenvalues of the four-level Hamiltonian (A4) for $\tilde{\Omega}_P=0$ and for $\Omega_S^{11}=\Omega_{\max}^{11}$, $\Omega_S^{21}=\Omega_{\max}^{21}$ where $\Omega_{\max}^{11}$ and $\Omega_{\max}^{21}$ are the maximum values of the Stokes Rabi frequencies for the transitions $3\,^3S_1\leftrightarrow 2\,^3P_1$ and $3\,^3S_1\leftrightarrow 2\,^3P_2$. In this case the eigenvalue that corresponds to the initial state $2\,^3S$ is $\varpi_N=-\hbar\tilde{\Delta}_1(t=t_{MS})/2$, where $t_{MS}$ is the time of the peak value of the Stokes pulse. To find the number $N$ of this state we calculate numerically the three other Stokes semidiabatic eigenvalues. Then we consider the pump semidiabatic eigenvalues, i.e., the eigenvalues of the Hamiltonian (A4) for $\tilde{\Omega}_P=\Omega_{\max}$ and for $\Omega_S^{11}=0$, $\Omega_S^{21}=0$ ($\Omega_{\max}$ is the maximum value of the pump Rabi frequencies for the transition $2\,^3S_1\leftrightarrow 3\,^3S_1$). They are $-\hbar\tilde{\Delta}_3/2$, $-\hbar\tilde{\Delta}_4/2$,

$$\hbar(\tilde{\Delta}_1+\tilde{\Delta}_2+\sqrt{(\tilde{\Delta}_1+\tilde{\Delta}_2)^2+4\Omega_{\max}^2})/4,$$

and

$$\hbar(\tilde{\Delta}_1+\tilde{\Delta}_2-\sqrt{(\tilde{\Delta}_1+\tilde{\Delta}_2)^2+4\Omega_{\max}^2})/4.$$

According to the peak-to-peak connectivity concept the eigenstate with the eigenvalue number $N$ from these four eigenvalues is connected with the initial state $2\,^3S_1$. Using the assumption of the diabatic evolution after the maximum of the pump pulse we find the bare state that is connected with the initial state.

The connectivity plot can be used to explain the experimental results shown on Fig. 7 and Fig. 8. Note that in the experiment the pump-laser intensity is radially inhomogeneous with maximum value, $I_P=80$ MW/cm$^2$. So we should use the connectivity plots calculated for some smaller average intensity. Figure 12 shows the connectivity regions for $M=\pm 1$ [Fig. 12(a)] and for $M=0$ [Fig. 12(b)] calculated for peak pulse intensities $I_P=55$ MW/cm$^2$ and $I_S=0.03$ MW/cm$^2$. The horizontal dot lines show intersections that correspond to the Stokes detunings from Fig. 7 and the vertical dot lines correspond to the pump detunings on Fig. 8. For example, on Fig. 7(a) a peak at $D_P\simeq -4.5$ GHz corresponds to STIHRAP to the $2p\ ^3P_2$ state for all magnetic sublevels, the second peak at $D_P\simeq -2.5$ GHz is due to STIHRAP to the $2p\ ^3P_1$ state for $M=\pm 1$. The third peak at $D_P\simeq 0$ GHz originated from population transfer to the upper $3s\ ^3S_1$ state followed by spontaneous emission to the target states. All other peaks in Fig. 7 and Fig. 8 can be explained similarly by examination of the intersections of the dotted lines with the filled regions on the connectivity plot in Fig. 12.

## V. CONCLUSION

We have demonstrated experimentally, with metastable helium, the successful coherent population transfer via the STIHRAP mechanism, whereby the pump excitation involves a two-photon transition. We confirmed that the effect of the dynamic Stark shifts induced by the pump laser can be partially compensated by choosing appropriate static detunings (pulse carrier frequency offsets from resonance). These detunings can be predicted theoretically. We achieved a transfer efficiency of 53% averaged over the spatial profile of the pump laser. In addition to detuning choices that allow high population transfer to the final state, we found that there exist other choices of static detunings that allow efficient population transfer to the intermediate state. This process is similar to SCRAP [11].

The experimental results are in good agreement with the numerical simulation of the system in the density-matrix formalism and with the analysis using adiabatic states. The sensitivity to detuning was demonstrated and shown to be in good agreement with theoretical connectivity considerations using the concept of semidiabatic peak-to-peak connectivity.

For practical application of the STIHRAP technique, for example in studies on reaction dynamics, there are two important conclusions. First, the process is very sensitive to the intensity of the pump laser. Power variations across the pump-laser beam are detrimental and have to be avoided in order to achieve uniform excitation everywhere in the molecular beam. Therefore it is necessary to work with large beam diameters, which requires high pulse energies to saturate the two-photon transition. Second, the process is very sensitive to the static detunings. In order to predict the set of detunings for good population transfer it is crucial to calculate the dynamic Stark shifts. For complicated molecular systems this may involve considerable theoretical effort.

## ACKNOWLEDGMENTS

We acknowledge support from the Deutsche Forschungsgemeinschaft and by the European Union Research and Training Network COCOMO, Contract No. HPRN-CT-1999-00129, as well as INTAS, Project No. 99-00019. L.P.Y., B.W.S., and K. Bergmann acknowledge support through the NATO collaborative research grant. B.W.S. acknowledges the support of ''Laserzentrum,'' University of Kaiserslautern. His work at Livermore was supported in part under the auspices of the U.S. Department of Energy at Lawrence Livermore National Laboratory under Contract No. W-7405-Eng-

48. L.P.Y. is grateful to the Deutsche Forschungsgemeinschaft for support of his visit to Kaiserslautern. We thank S. Guérin, Université de Bourgogne, Dijon, and E. E. Eyler, University of Connecticut, for helpful discussions on the topic.

## APPENDIX: NUMERICAL SIMULATION

The time evolution of the population in the 15 magnetic sublevels is computed by numerically integrating the Liouville equation for the density matrix $\rho$

$$\frac{d\rho}{dt} = -\frac{i}{\hbar}[H,\rho] + \dot{\rho}_{relax} + \dot{\rho}_{exc}. \tag{A1}$$

The relaxation and excitation matrices are defined by

$$[\dot{\rho}_{relax}]_{ij} = -\frac{1}{2}(\gamma_i + \gamma_j)\rho_{ij}, \quad [\dot{\rho}_{exc}]_{ij} = \delta_{ij}\sum_k A_{kj}\rho_{kk}, \tag{A2}$$

where $\gamma_i$ is the decay rate of level $i$ and $A_{ij}$ is the Einstein coefficient for the transition $i \rightarrow j$. The coefficients $A_{ij}$ for the individual magnetic sublevels were calculated from the overall decay rates listed in [12] by using the square of the respective Clebsch-Gordan coefficient

$$|\langle J\,1\,M\,\Delta M \,|\, J\,1\,J'\,M'\rangle|^2.$$

The rotating-wave approximation Hamiltonian has the block structure

$$H = \begin{pmatrix} H^{(1)} & & & \\ & H^{(2)} & & \\ & & H^{(3)} & \\ & & & H^{(4)} \end{pmatrix} \tag{A3}$$

with

$$H^{(1)} = -\frac{\hbar}{2}\begin{pmatrix} \tilde{\Delta}_1 & \tilde{\Omega}_P & 0 & 0 \\ \tilde{\Omega}_P & \tilde{\Delta}_2 & \Omega_S^{1\,1} & \Omega_S^{2\,1} \\ 0 & \Omega_S^{1\,1} & \tilde{\Delta}_3 & 0 \\ 0 & \Omega_S^{2\,1} & 0 & \tilde{\Delta}_4 \end{pmatrix}, \tag{A4}$$

$$H^{(2)} = -\frac{\hbar}{2}\begin{pmatrix} \tilde{\Delta}_5 & \tilde{\Omega}_P & 0 & 0 \\ \tilde{\Omega}_P & \tilde{\Delta}_6 & \Omega_S^{0\,0} & \Omega_S^{2\,0} \\ 0 & \Omega_S^{0\,0} & \tilde{\Delta}_7 & 0 \\ 0 & \Omega_S^{2\,0} & 0 & \tilde{\Delta}_8 \end{pmatrix}, \tag{A5}$$

$$H^{(3)} = -\frac{\hbar}{2}\begin{pmatrix} \tilde{\Delta}_9 & \tilde{\Omega}_P & 0 & 0 \\ \tilde{\Omega}_P & \tilde{\Delta}_{10} & \Omega_S^{1\,1} & \Omega_S^{2\,1} \\ 0 & \Omega_S^{1\,1} & \tilde{\Delta}_{11} & 0 \\ 0 & \Omega_S^{2\,1} & 0 & \tilde{\Delta}_{12} \end{pmatrix}, \tag{A6}$$

and

$$H^{(4)} = -\frac{\hbar}{2}\begin{pmatrix} \tilde{\Delta}_{13} & 0 & 0 \\ 0 & \tilde{\Delta}_{14} & 0 \\ 0 & 0 & \tilde{\Delta}_{15} \end{pmatrix}. \tag{A7}$$

The indices of the levels are chosen as indicated by the encircled numbers in Fig. 2. The two-photon pump Rabi frequency is denoted by $\tilde{\Omega}_P$, the Stokes Rabi frequencies $\Omega_S^{J\,|M|}$ are labeled with the quantum numbers $J$ and $M$ of the respective target level of the $2\,^3P$ state and the Stark shift of state $i$ is denoted by $S_i$. The values are listed in Table I. Here we have the special case $\Omega_S^{1\,1} = \Omega_S^{2\,1}$.

The angular frequencies $\omega_P$ and $\omega_S$ denote the carrier frequencies of the pump and Stokes laser fields. The static pump detuning is given by $\Delta_P = \omega_{3s} - \omega_{2s} - 2\omega_P$, where $\omega_i = E_i/\hbar$ is related to the energy $E_i$ of the respective state. We define the static Stokes detunings as $\Delta_S^J = \omega_{3s} - \omega_{2p,J} - \omega_S$ (for example, $\Delta_S^0$ is zero for resonance with the $3\,^3\mathrm{S} \leftarrow 2\,^3P_0$ transition). The experimental detunings $D_P$ and $D_S$ in Sec. III are given in units of frequency and have opposite sign. The relation to the detunings used here (in units of angular frequency) is $-4\pi D_P = \Delta_P$ and $-2\pi D_S = \Delta_S^1$. The energy spacings [13] of the $J=1$ and $J=2$ levels with respect to the $J=0$ level are denoted by $\Delta\omega_1 = \omega_{J=0} - \omega_{J=1}$ and $\Delta\omega_2 = \omega_{J=0} - \omega_{J=2}$ (see Fig. 2). The dynamically shifted detunings (compare paper II, $\tilde{\Delta}_S^{J\,|M|}$ denotes the Stokes detuning with respect to the magnetic sublevel with quantum numbers $J$ and $M$ of the $2\,^3P$ state)

$$\begin{aligned}
\tilde{\Delta}_P &= \Delta_P + S_2 - S_1, \\
\tilde{\Delta}_S^{0\,0} &= \Delta_S^0 + S_6 - S_7, \\
\tilde{\Delta}_S^{1\,1} &= \Delta_S^0 + \Delta\omega_1 + S_2 - S_3, \\
\tilde{\Delta}_S^{2\,1} &= \Delta_S^0 + \Delta\omega_2 + S_2 - S_4, \\
\tilde{\Delta}_S^{2\,0} &= \Delta_S^0 + \Delta\omega_2 + S_6 - S_8,
\end{aligned}$$

lead to the following expressions for the diagonal elements $\tilde{\Delta}_i$:

$$\begin{aligned}
&\tilde{\Delta}_1 = \tilde{\Delta}_P - \tilde{\Delta}_S^{1\,1}, \quad \tilde{\Delta}_2 = -\tilde{\Delta}_P - \tilde{\Delta}_S^{1\,1}, \\
&\tilde{\Delta}_3 = -\tilde{\Delta}_1, \quad \tilde{\Delta}_4 = -\tilde{\Delta}_P - \tilde{\Delta}_S^{1\,1} + 2\tilde{\Delta}_S^{2\,1}, \\
&\tilde{\Delta}_5 = \tilde{\Delta}_P - \tilde{\Delta}_S^{0\,0}, \quad \tilde{\Delta}_6 = -\tilde{\Delta}_P - \tilde{\Delta}_S^{0\,0}, \\
&\tilde{\Delta}_7 = -\tilde{\Delta}_5, \quad \tilde{\Delta}_8 = -\tilde{\Delta}_P - \tilde{\Delta}_S^{0\,0} + 2\tilde{\Delta}_S^{2\,0}, \\
&\tilde{\Delta}_9 = \tilde{\Delta}_1, \quad \tilde{\Delta}_{10} = \tilde{\Delta}_2, \\
&\tilde{\Delta}_{11} = -\tilde{\Delta}_1, \quad \tilde{\Delta}_{12} = \tilde{\Delta}_4,
\end{aligned} \tag{A8}$$

The detunings $\tilde{\Delta}_{13}, \tilde{\Delta}_{14}$ and $\tilde{\Delta}_{15}$ of the levels that are not coupled are arbitrary. We set them to zero.

In the simulation we use Gaussian pulses given by

$$I_P(t) = I_P^0 \exp[-4\ln(2)\, t^2/\tau_{1/2}^2] \tag{A9}$$

$$I_S(t) = I_S^0 \exp[-4\ln(2)\,(t-\Delta\tau)^2/\tau_{1/2}^2], \tag{A10}$$

where the pulse delay $\Delta\tau$ is positive when the Stokes pulse follows the pump pulse. The full width of the laser pulses at half maximum of intensity is $\tau_{1/2} = 4.9$ ns.


[1] K. Bergmann, H. Theuer, and B. W. Shore, Rev. Mod. Phys. **70**, 1003 (1998).

[2] J. Martin, B. W. Shore, and K. Bergmann, Phys. Rev. A **54**, 1556 (1996).

[3] T. Halfmann and K. Bergmann, J. Chem. Phys. **104**, 7068 (1996).

[4] A. Kuhn, S. Steuerwald, and K. Bergmann, Eur. Phys. J. D **1**, 57 (1998).

[5] S. Schiemann, A. Kuhn, S. Steuerwald, and K. Bergmann, Phys. Rev. Lett. **71**, 3637 (1993).

[6] U. Czarnetzki, U. Wojak, and H. F. Döbele, Phys. Rev. A **40**, 6120 (1989).

[7] L. P. Yatsenko, S. Guérin, T. Halfmann, K. Böhmer, B. W. Shore, and K. Bergmann, Phys. Rev. A **58**, 4683 (1998).

[8] S. Guérin, L. P. Yatsenko, T. Halfmann, B. W. Shore, and K. Bergmann, Phys. Rev. A **58**, 4691 (1998).

[9] L. P. Yatsenko, T. Halfmann, B. W. Shore, and K. Bergmann, Phys. Rev. A **59**, 2926 (1999).

[10] T. Halfmann, J. Koensgen, and K. Bergmann, Meas. Sci. Technol. **11**, 1510 (2000).

[11] T. Rickes, L. P. Yatsenko, S. Steuerwald, T. Halfmann, B. W. Shore, N. V. Vitanov, and K. Bergmann, J. Chem. Phys. **113**, 534 (2000).

[12] W. C. Wiese, M. W. Smith, and B. M. Glennon, Natl. Stand. Ref. Data Ser. (U.S., Natl. Bur. Stand.) **4**, 1 (1966).

[13] W. C. Martin, Phys. Rev. A **36**, 3575 (1987).